Nanoscale Res Lett (2007) 2:561–568
DOI 10.1007/s11671-007-9099-8

NANO EXPRESS

Excitonic Transitions and Off-resonant Optical Limiting in CdS Quantum Dots Stabilized in a Synthetic Glue Matrix

Pushpa Ann Kurian · C. Vijayan · K. Sathiyamoorthy · C. S. Suchand Sandeep · Reji Philip

Received: 1 August 2007 / Accepted: 5 October 2007 / Published online: 25 October 2007

Abstract Stable films containing CdS quantum dots of mean size 3.4 nm embedded in a solid host matrix are prepared using a room temperature chemical route of synthesis. CdS/synthetic glue nanocomposites are characterized using high resolution transmission electron microscopy, infrared spectroscopy, differential scanning calorimetry and thermogravimetric analysis. Significant blue shift from the bulk absorption edge is observed in optical absorption as well as photoacoustic spectra indicating strong quantum confinement. The exciton transitions are better resolved in photoacoustic spectroscopy compared to optical absorption spectroscopy. We assign the first four bands observed in photoacoustic spectroscopy to $1s_e$–$1s_h$, $1p_e$–$1p_h$, $1d_e$–$1d_h$ and $2p_e$ –$2p_h$ transitions using a non interacting particle model. Nonlinear absorption studies are done using z-scan technique with nanosecond pulses in the off resonant regime. The origin of optical limiting is predominantly two photon absorption mechanism.

Keywords Exciton · Nanomaterials · Optical limiting · Nonlinearity · Photoacoustics

Introduction

Semiconductor nanocrystals have been receiving considerable attention over the past several years as model systems exhibiting quantum confinement effects and hence as potential candidate materials for device applications such as optical limiting and optical switching [1–6]. Optical limiting has been reported for semiconductor doped glasses [1, 2] and semiconductor nanoparticle solutions [4, 5]. An area of recent focus has been the development of simple and efficient methods of synthesis for obtaining these materials in a stable and device-friendly form in large quantities where synthesis of nanocrystals in a polymer host plays an important role [7, 8]. Nanocrystals embedded in solid polymer films have the advantages of transparency and high optical, thermal, and chemical stability apart from low cost, reproducibility and ease of preparation. The composite films retain the optical properties of the nanocrystals while providing a convenient matrix and remain stable for considerably longer durations compared to those dispersed in solutions.

Cadmium sulphide is a direct bandgap II–VI semiconductor material with a bulk band gap of 2.38 eV and exciton Bohr radius of 3 nm. Bulk CdS is known to be a very good nonlinear optical material [9]. Semiconductor nanocrystals of size comparable to bulk exciton radius are known to exhibit excitonic features arising from discretization of the band edge due to strong quantum confinement [10, 11]. The excitonic features in the absorption and luminescence spectra show significant blue shift with decreasing particle size, making the optical properties size dependent [12].

Knowledge of the electronic transitions is essential in understanding the linear and nonlinear optical properties of these materials. The spectroscopic techniques used for the investigation of energy levels are mostly optical absorption, photoluminescence and Raman spectroscopy [13–16], which have provided considerable insight into the excitonic transitions. Another form of spectroscopy that could be used effectively to gather better resolved spectral

P. A. Kurian · C. Vijayan (✉) · K. Sathiyamoorthy
Indian Institute of Technology Madras, Chennai 600036, India
e-mail: cvijayan@physics.iitm.ac.in

C. S. Suchand Sandeep · R. Philip
Raman Research Institute, Bangalore 560080, India

information is photoacoustic spectroscopy (PAS), particularly in the case of samples such as polymer-stabilized CdS nanocrystals where nonradiative transitions dominate and luminescence gets quenched. This technique is used in the present work for probing the electronic transitions in CdS quantum dots and correlating the observed data with the theoretical transitions obtained from a noninteracting particle model.

Optical nonlinearties have been studied using different experimental techniques like degenerate four wave mixing (DFWM), z-scan technique, optical interferometry and nonlinear absorption. Reports are available on large nonlinearities observed in CdS nanocrystals using DFWM and pump probe experiments [17–21] and also on the relaxation dynamics of these materials using femtosecond time resolved pump probe and photoluminescence studies [22, 23]. Recently He et al. [24] studied two photon absorption and Kerr nonlinearity of CdS nanocrystals synthesized by ion exchange method in Nafion film using pump probe and optical Kerr effect techniques with 350 fs pulses at 800 nm. The z-scan technique can give information regarding both nonlinear refraction and nonlinear absorption. Most of the work done on the nonlinear optical properties of semiconductor nanocrystals are on semiconductor doped glasses. One major limitation of semiconductor doped glasses is the photodarkening effect. A few reports are there on the nonlinear optical properties of semiconductor nanocrystals suspended in solutions. The volume fraction of nanocrystals in solutions is usually small resulting in weak nonlinear response. Thus, polymer-embedded nanomaterials appear to be better candidate materials for the study of nonlinear optical response.

Nonlinear refraction has been studied in CdS nanocrystals incorporated in polydiacetylene [25] and polystyrene [26] using nanosecond pulses in the near resonant regime. It is well known that resonant nonlinearity is large but has a slow response with large linear absorption. On the other hand, off resonant nonlinearity has ultrafast response. Semiconductor nanocrystals with large nonlinearity are also known to be attractive candidate materials for optical limiting. Optical limiters are devices which have constant transmittance at low input fluences and a decrease in transmittance at high fluences. These devices are used to protect optical sensors and eyes from laser induced damage.

We have synthesized a nanocomposite material incorporating strongly confined CdS nanocrystals of average size 3.4 nm stabilized in a synthetic glue matrix. The samples are free standing films with good optical quality and photostability. The excitonic transitions are studied using optical and photoacoustic spectroscopy and the results are correlated with a non interacting particle model. PAS studies show that the energy corresponding to the first excitonic transition is $E_g = 2.69$ eV. Further, we have also investigated strong absorptive nonlinearity excited by nanosecond laser pulses in the off resonant regime $(E_g > \hbar\omega > E_g/2)$ at 532 nm. The observed optical limiting behavior is discussed on the basis of two photon absorption process.

Experimental Section

The method of synthesis used for the present work is based on a chemical route for preparing PbS nanocomposite films reported by us recently [27]. The precursors used are cadmium acetate and sodium sulphide of analytic grade. A commercially available, transparent, water soluble poly(vinyl acetate) (PVAc) glue purchased from Crown Chemicals Chennai, India is used as the host matrix to prepare the nanocomposite. The samples are prepared by processing equimolar quantities of sodium sulphide and cadmium acetate in the glue medium, stirring continuously. The solution was poured into petridishes and air dried to obtain stable optical quality films. The concentrations of cadmium acetate used are 0.5, 1, 2 and 3 mM in 50 ml aqueous solution of the glue. The four samples corresponding to these four different concentrations are designated as C1, C2, C3 and C4 respectively. The concentration of sodium sulphide used in each case is such that an equimolar ratio of Cd^{2+}:S^{2-} is obtained in all cases. The composite films are found to be very stable and they retain their physical properties for long periods of time. The thickness of the films used in the present study is 126 μm.

The morphological characterization is done using a Jeol 3010 high resolution transmission electron microscope with an accelerating voltage of 300 kV. The IR spectrum is recorded with a Perkin Elmer Spectrum One Fourier transform infrared (FTIR) spectrophotometer to obtain information about the surface of the nanocrystal.

Thermogravimetric analysis are performed using a Perkin Elmer Pyris 6 thermogravimetric analyzer (TGA). Thermal decompositions are recorded between 30 °C and 900 °C. The heating rate is 10 °C min^{-1}. The differential scanning calorimetry (DSC) studies are done with a NETZSCZ DSC (200 Phox). The experiments are performed under a nitrogen atmosphere. The heating rate is 10 °C min^{-1}.

Optical absorption spectra are recorded on a Jasco V-570 spectrometer in the wavelength region 300 nm–600 nm in which the host matrix is transparent. The photoacoustic spectroscopic studies are done by the gas microphone technique [28]. The spectrum is recorded using an automated home-built photoacoustic spectrometer. A xenon arc lamp of 500 W is used as the excitation source. The light beam is passed through a monochromator

(Jobin Yvon), modulated using a mechanical chopper (SR540, Stanford research systems) and focused to an airtight photoacoustic (PA) cell. The modulation frequency is 10 Hz. The PA cell consists of an aluminium cylinder with an option for inserting a microphone in its periphery. The periodically chopped beam is allowed to fall on the sample kept inside the PA cell through the transparent cell window. The nonradiative transitions within the sample heat up the boundary layer of air in contact with the sample. The periodic heating effect causes the layer to function as a vibrating piston. This results in periodic pressure fluctuations inside the cell which are detected by the sensitive microphone (G.R.A.S). The amplitude and phase angle of the PA signal are finally detected by a lock in amplifier (SR830, Stanford research systems) whose reference channel is connected from the chopper. The spectral measurements are carried out at room temperature in the wavelength range of 360–600 nm in steps of 2 nm. The PA spectrum is corrected for variations in source intensity as a function of wavelength using carbon black absorber for normalization. The nonlinear absorption studies are done by the z-scan technique [29] using 7 ns pulses from a Nd-YAG laser emitting at the second harmonic wavelength of 532 nm. The spatial intensity profile of the laser is found to be near Gaussian by beam profile measurements using the knife edge method. An automated open aperture z-scan set up is used to measure intensity dependent transmission. The laser beam is focused using a lens of focal length 185 mm and the transmittance is measured using a pyroelectric energy probe as a function of sample position z by translating the sample along the beam axis (z-axis). The sample sees a different fluence at each position of z. The small fluctuations in the pulse energy are accounted for by using a reference energy probe. The pulse-to-pulse energy stability is found to be approximately 5%. Depending on the absorption mechanism involved, we get a Lorentzian or inverted Lorentzian with its maximum or minimum at the focal point, z = 0 where the fluence is a maximum.

Results and Discussion

Embedding nanocrystallites in stable, transparent solid matrices is important from the point of view of the nature of cluster-host interaction whereas it also renders the sample in a convenient form for potential applications. The search for convenient and economic procedures of synthesis to achieve this has hence been of frontier interest. Most of the earlier methods for the synthesis of embedded II–VI nanocrystals were in glass matrix and involved procedures such as high temperature melting and annealing and the resulting size distribution of the clusters was rather broad. On the other hand, the main advantage of synthesis of nanocrystals in polymer matrices is the low temperature procedure, at not more than 200 °C. The motivation for the present work is to explore a much simpler and economic procedure of embedding nanocrystals in a stable and transparent matrix. The method we adopted here for the synthesis of CdS nanocrystals based on the chemical replacement reaction between Cd^{2+} ions and S^{2-} ions in a synthetic glue matrix is a room temperature synthesis. Within a few seconds of addition of sodium sulphide into the aqueous solution of glue matrix containing cadmium acetate salt, CdS nanocrystals are formed.

The CdS-synthetic glue composites have wide processing flexibility enabling us to make coatings of nanometer thickness, fibres and films depending on the requirement. Major challenge in the nanoparticle synthesis is to produce small size stable nanoparticles (to prevent agglomeration) with reproducibility. Synthetic glue matrix is found to be an excellent matrix overcoming these difficulties with an efficient dispersion of nanoparticles.

Characterization by HRTEM, TEM, FTIR, DSC and TGA

Figure 1 shows the HRTEM picture of a single CdS nanocrystal embedded in the matrix (sample C4). The crystallographic planes can be seen clearly in the region corresponding to the nanocrystal. The micrograph shows that the quasi spherical CdS nanocrystals are homogenously dispersed and well separated in the host matrix. Size distribution of the nanocrystals is found to be 3–5.7 nm with majority of the nanocrystals in the 3 nm size range. The mean size of 3.4 nm is determined by evaluating 290 particles.

The role of polymer molecules on the surface physics of the nanocrystals is probed by the technique of FTIR spectroscopy. The FTIR spectrum of the host matrix is shown in Fig. 2a. The prominent peaks observed at 1735 cm^{-1} ($\nu_{C=O}$), 1095 cm^{-1}, 1263 cm^{-1} (ν_{C-O}) and 1376 cm^{-1} (δ_{CH3}) confirm the presence of poly(vinyl acetate) (PVAc). The spectrum is similar to the standard IR spectrum of PVAc. (Sprouse collection of IR, card no.187–189). The peak at 1711 cm^{-1} in the FTIR spectrum of the CdS embedded glue (sample C4) (Fig. 2b) corresponds to the C=O stretching frequency whereas in the host glue matrix the C=O stretching frequency is at 1735 cm^{-1} . This decrease in stretching frequency can be attributed to interaction of metal ion with the C=O group. When cadmium acetate is added to the aqueous solution of glue, Cd^{2+} ions are homogeneously dispersed in the matrix. The –C=O groups present in the polymer side chain interact with the Cd^{2+} ions and stabilize it. On the addition of aqueous

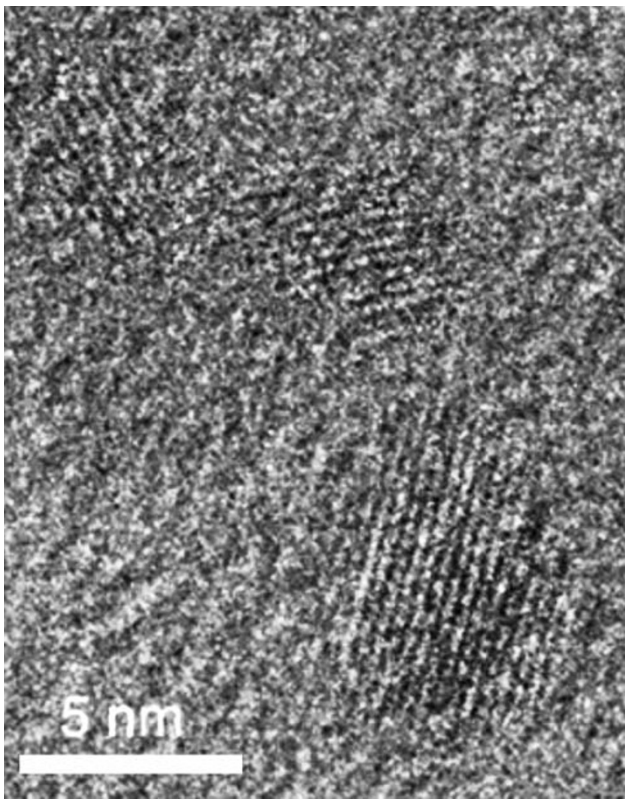

Fig. 1 HRTEM image showing well dispersed CdS nanocrystals in synthetic glue matrix

solution of Na_2S, Cd^{2+} ions in the host matrix react with S^{2-} forming CdS. The CdS nanocrystals thus formed are surrounded by the polymer chains, preventing further diffusion of CdS nanocrystals and thus controlling the growth process at room temperature.

Differential scanning calorimetry (DSC) experiments (figures not shown) indicate that the glass transition temperature (T_g = 52.9 °C) remains the same for the host glue matrix and the CdS nanocrystals embedded host matrix. This shows that the physical properties of the polymer are retained even after the in-situ formation of CdS nanocrystals. Figure 3 shows the thermograms of synthetic glue host matrix and CdS/glue nanocomposite (sample C4) obtained under air atmosphere. The onset temperature (corresponding to a loss of 10 mass%) is found to be the same, 270 °C, for both the host matrix as well as CdS-incorporated host matrix. A more accurate measure of the thermal stability of a material is T_o, the temperature corresponding to the maximum weight loss rate $(dm/dT)_{max}$ in the first decomposition reaction. This temperature is found to be 314 °C for both the host matrix and the CdS/glue nanocomposite, indicating that the presence of CdS nanocrystals does not affect the thermal stability of the host matrix.

Optical Absorption and Photoacoustic Spectra

Figure 4 shows the optical absorption spectra (OAS) of CdS nanocrystals in glue matrix of samples C1, C2, C3 and C4. The host matrix shows no absorption in the wavelength range under consideration. Second derivative of the optical absorption spectrum indicates that the absorption onset is at 2.64 eV. The spectrum shows a considerable blueshift from the bulk absorption onset of 2.38 eV.

The optical absorption spectra of semiconductor nanocrystals are known to show a blueshifted absorption onset with features due to exciton absorption, as observed in the present work, from which it is difficult to get detailed information about the exciton transitions. On the other hand, a more direct measurement of the spectral features of the absorbed energy can be obtained from PAS which enables to observe better resolved bands. This is because large optical density and scattering from the sample tend to make the signal to noise ratio poor in the case of the optical absorption experiment where it is the intensity of the

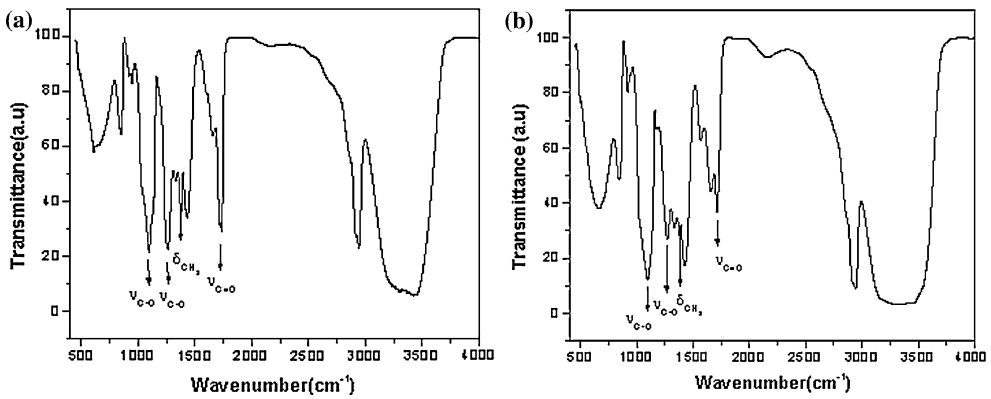

Fig. 2 FTIR spectrum of (**a**) PVAc glue matrix (**b**) CdS/Glue nanocomposite

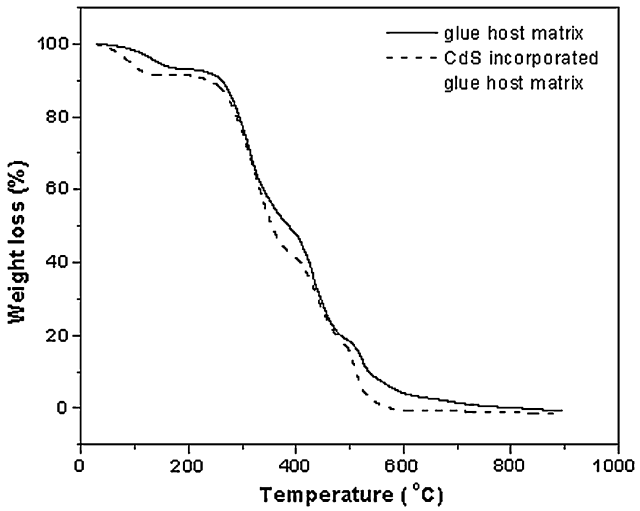

Fig. 3 TGA curves for glue matrix (solid line) and CdS/Glue nanocomposite (dashed line)

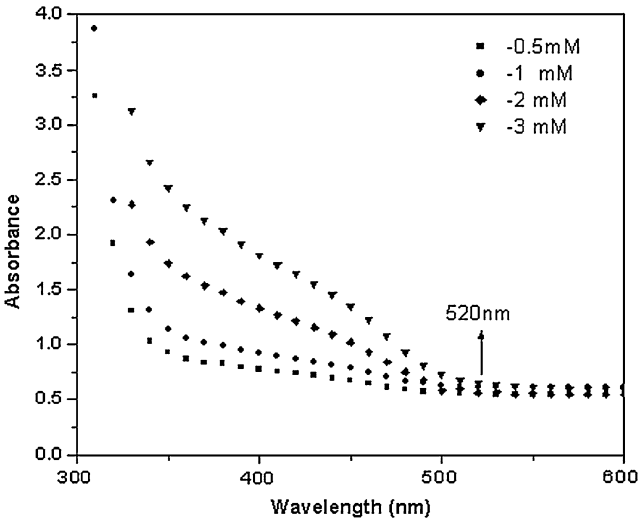

Fig. 4 Optical absorption spectra of CdS/Glue nanocomposite films of different concentrations

transmitted beam that is measured. However, these factors do not cause any problem to the photoacoustic response of the sample. Hence we measured the photoacoustic response of the samples in a home made PA spectrometer.

Figure 5a shows the photoacoustic spectra of CdS nanocrystals in host matrix. The photoacoustic spectrum (PAS) of the host matrix is featureless in the wavelength range under consideration. Figure 5b shows PAS of sample C4. The spectrum shows a multipeak structure. The spectrum is analysed using a curve fitting program assuming Gaussian line shape. The analysis yields four peaks at 2.69 eV (denoted as E1 band), 2.81 eV (E2 band), 2.96 eV (E3 band) and 3.21 eV (E4 band). The full width at half maximum (FWHM) of first excitonic transition obtained from PAS is 0.14 eV, in good agreement with that of the first excitonic transition obtained from optical absorption spectroscopy.

The mean diameter of the nanocrystals in the present study is 3.4 nm, corresponding to the regime of strong confinement, where Coulomb interaction effects can be neglected [11]. So we use a non interacting particle model (NIP) [10, 30] to assign the four bands obtained from photoacoustic spectroscopy. NIP is based on effective mass approximation (EMA) model where Coulomb interaction of the electron-hole pair is neglected. Therefore the exciton Hamiltonian can be written as

$$H = -\frac{h^2}{8\pi^2 m_e}\nabla_e^2 - \frac{h^2}{8\pi^2 m_h}\nabla_h^2 + V_e(r_e) + V_h(r_h) \quad (1)$$

where the first two terms on the R.H.S are the kinetic energies of the electron and hole respectively, V_e and V_h are the potentials experienced by the electron and hole respectively due to the barrier and m_e and m_h are the effective masses respectively. The confinement potential may be defined as

$$V_i(r_i) = 0 \text{ for } r_i < R$$
$$= \infty \text{ for } r_i > R \ (i = e, h)$$

where R is the radius of the spherical nanocrystal.

In this model, hole and electron energy levels in the nanocrystal can be expressed as

$$E_{n,l}^h = \frac{-\hbar^2 \xi_{n,l}^2}{2m_h R^2} \quad (2)$$

and

$$E_{n,l}^e = E_g + \frac{\hbar^2 \xi_{n,l}^2}{2m_e R^2} \quad (3)$$

where $\xi_{n,l}$ is the nth zero of the spherical Bessel function.

Optical transitions will occur at energies

$$\hbar\omega = E_g + E_{n,l}^e - E_{n,l}^h = E_g + \frac{h^2}{8\pi^2 m_r}\left[\frac{\xi_{n,l}^2}{R^2}\right] \quad (4)$$

where m_r is the reduced effective mass of the electron-hole pair,

$$\frac{1}{m_r} = \frac{1}{m_e} + \frac{1}{m_h} \quad (5)$$

Theoretical models such as EMA and tight binding (TB) model tend to overestimate the exciton transition energies in nanocrystals of smaller diameter compared to the transition energies obtained from the experimental results [31–33]. At the same time, both theory and experiment agree well in the case of nanocrystals of larger diameters. In the case of smaller nanocrystals the disagreement between theory and experiment may be due to using bulk

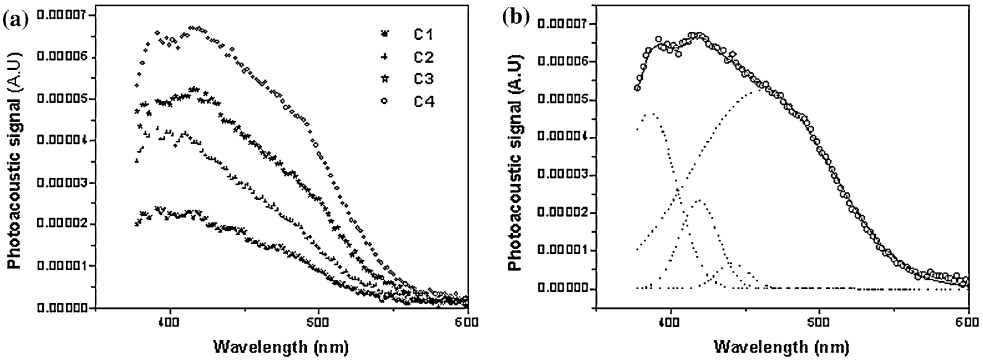

Fig. 5 (**a**) Photoacoustic spectra of CdS/Glue nanocomposite films (**b**) Photoacoustic spectrum of CdS/Glue nanocomposite (circles) along with Gaussian fit (solid line). Deconvoluted peaks corresponding to excitonic transitions (dashed lines)

material parameters such as effective mass and bandgap as numerical inputs to the theory. The main advantage of this method of analysis, used in the present work and proposed for the first time by Nandakumar et al [13], is that it eliminates the use of bulk parameters in the calculation. Including Coloumb interaction into the calculations would make the analysis more complete, though it has not been taken up as part of the present work in view of the strong confinement.

Nandakumar et al. have used photoacoustic spectroscopy to analyze the electronic transitions in CdS nanocrystals and presented [12, 34] a comparison between the experimental and theoretical determination of transition energies in which the bulk material parameters such as effective masses and bulk bandgap E_g are eliminated. We have followed this procedure to assign the four bands observed in PAS. Using NIP model for spherical quantum dots, the first few transitions are calculated and labeled as T1, T2 etc. as shown in Table 1. In this analysis, the difference between electron and hole energies corresponding to the transitions $1s_e$–$1s_h$, $1p_e$–$1p_h$, $1d_e$–$1d_h$ etc. (Table 1) eliminates the bulk bandgap E_g. The differences in transitions are calculated in Table 2. The ratio of the differences in transitions calculated as shown in Table 3 eliminates effective masses m_e and m_h and nanocrystal radius R. The theoretical ratios are then compared with ratios obtained experimentally (Table 3). The theoretical ratios and experimental ratios agree well if we assign the first four bands observed in PAS to $1s_e$–$1s_h$ (band E1), $1p_e$–$1p_h$ (band E2), $1d_e$–$1d_h$ (band E3) and $2p_e$–$2p_h$ (band E4).

Table 1 First few transition energies calculated for spherical quantum dots using noninteracting particle model

Level	Transition	$\xi_{n,l}$	δE
T1	$1s_e$–$1s_h$	3.1416	$\frac{(3.1416)^2}{m_r}\frac{\hbar^2}{8\pi^2R^2}$
T2	$1p_e$–$1p_h$	4.4934	$\frac{(4.4934)^2}{m_r}\frac{\hbar^2}{8\pi^2R^2}$
T3	$1d_e$–$1d_h$	5.7635	$\frac{(5.7635)^2}{m_r}\frac{\hbar^2}{8\pi^2R^2}$
T4	$2s_e$–$2s_h$	6.2832	$\frac{(6.2832)^2}{m_r}\frac{\hbar^2}{8\pi^2R^2}$
T5	$2p_e$–$2p_h$	7.7523	$\frac{(7.7253)^2}{m_r}\frac{\hbar^2}{8\pi^2R^2}$
T6	$2d_e$–$2d_h$	9.0950	$\frac{(7.7253)^2}{m_r}\frac{\hbar^2}{8\pi^2R^2}$

Optical Limiting Studies

The samples are found to exhibit large optical nonlinearity, leading to optical limiting behavior. The nonlinearity is probed using the z-scan technique. Optical limiting can be due to a variety of nonlinear optical processes such as self focusing, self defocusing, nonlinear scattering and nonlinear absorption. Optical limiters based on nonlinear absorption mechanisms like free carrier absorption and multiphoton absorption are very efficient. Open z-scan studies are done to investigate the nonlinear absorption mechanism responsible for the observed optical limiting. The z-scan experiment is performed with the samples C1, C2, C3 and C4. For the samples C1 and C2, the concentration was not sufficient to show optical nonlinearity. Figure 6a and b show the optical limiting curves for sample C3 and C4 respectively. The optical limiting curves are extracted from open z-scan data. Transmission values are normalized to the value obtained for the lowest input

Table 2 Difference between transition energies corresponding to $1s_e$–$1s_h$, $1p_e$–$1p_h$, $1d_e$–$1d_h$, $2s_e$–$2s_h$, $2p_e$–$2p_h$, $2d_e$–$2d_h$ (Table 1)

Transition differences	Energy in units of $\frac{\hbar^2}{8\pi^2R^2m_r}$
T2–T1	$(4.4934^2 - 3.1416^2)$
T3–T2	$(5.7635^2 - 4.4934^2)$
T4–T2	$(6.2832^2 - 4.4934^2)$
T5–T2	$(7.7253^2 - 4.4934^2)$
T6–T2	$(9.0950^2 - 4.4934^2)$

Table 3 The ratio of the differences in transition energies calculated theoretically and experimentally

Theoretical values		Experimental values	
$\frac{T3-T2}{T2-T1}$	1.262	$\frac{E3-E2}{E2-E1}$	1.25
$\frac{T4-T2}{T2-T1}$	1.869		
$\frac{T5-T2}{T2-T1}$	3.827	$\frac{E4-E2}{E2-E1}$	3.33
$\frac{T6-T2}{T2-T1}$	6.059		

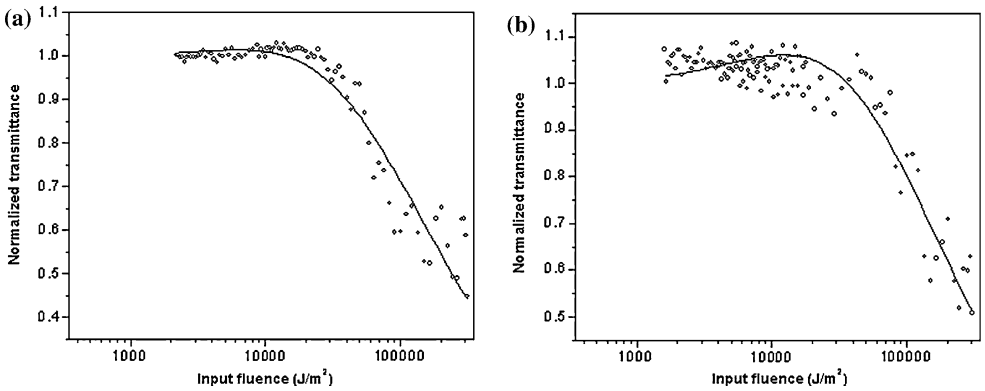

Fig. 6 Normalized transmittance of the samples C3 (**a**) and C4 (**b**) at an excitation intensity 4.33×10^9W/cm^2 as a function of the input fluence. Solid line is a numerical fit to the experimental data using Eq. (7)

fluence, which is taken as unity. The circles denote the experimental data and solid line denotes the theoretical fit. Since the wavelength chosen for the study is in the off resonant regime where the photon energy 2.33 eV is less than the fundamental absorption edge 2.69 eV, the experimental data are analysed using a model incorporating saturable absorption followed by two photon absorption (2PA). We consider a nonlinear absorption coefficient of the form [35]

$$\alpha(I) = \frac{\alpha_o}{1 + \frac{I}{I_s}} + \beta I \tag{6}$$

where α_o is the linear absorption coefficient, β is the 2PA coefficient, I is the laser intensity and I_s is the saturation intensity. Therefore the modified normalized transmittance using Eq. (6) can be written as

$$T(z) = \frac{Q(z)}{\sqrt{\pi} q(z)} \int_{-\infty}^{\infty} \ln[1 + q(z) \exp(-\tau^2)] d\tau \tag{7}$$

where $Q(z) = \exp(\alpha_o L I/(I + I_s))$, $q(z) = \beta I_o L_{eff}/1 + (z/z_o)^2$ with I_o being the peak intensity at the focal point and $L_{eff} = [1 - \exp(-\alpha_o L)]/\alpha_o$ where L is the sample length and $z_o = \pi\omega_o^2/\lambda$, where ω_o is the beam waist and λ is the wavelength of the exciting light.

The experimental data and theoretical fit are in good agreement, indicating that the mechanism of nonlinear absorption here is 2PA. The values of β and I_s are found to be $\beta = 1.9 \times 10^{-9}$ m/W and $I_s = 2.3 \times 10^{12}$ W/m^{-2} respectively, at 4.33×10^9 W/cm^2 (corresponding to laser energy 80 μJ) for both the samples C3 and C4 indicating there is no accumulative optical nonlinearity with the increase in concentration. Eventhough TPA appears to be the predominant mechanism, free carrier absorption also could be operative. The absorption spectrum shows a long wavelength tail absorption which can be due to the defect levels arising from sulphur vacancies which are located below the conduction band in bulk CdS [36]. The evidence for this defect level emission in CdS nanocrystals has been reported previously [12, 37]. So, when excited with a photon of energy 2.33 eV, the carriers may get excited to this defect level and free carrier absorption from these levels may happen as the experiments are done with pulses of nanosecond duration.

Conclusion

Free standing films of CdS quantum dots of mean size 3.4 nm are synthesized by a simple chemical route using synthetic glue as the host matrix. The excitonic transitions are studied using photoacoustic spectroscopy and analyzed in detail using noninteracting particle model. We assign the first four bands observed in PAS to $1s_e$–$1s_h$ (band E1), $1p_e$–$1p_h$ (band E2), $1d_e$–$1d_h$ (band E3) and $2p_e$–$2p_h$ (band E4). The origin of the optical limiting behavior is probed using z-scan technique with nanosecond laser pulses in the off resonant regime $(E_g > \hbar\omega > E_g/2)$ at 532 nm. The experimental data are analysed using a model incorporating saturable absorption followed by two photon absorption. The optical limiting behaviour is found to be predominantly due to two photon absorption process. Nanocomposite films in the present work have the advantages of large optical nonlinearity and transparency apart from low cost, reproducibility and ease of preparation. They also have high optical, thermal, and chemical stability and hence render the nanocrystals in form convenient for device applications.

Acknowledgments Financial assistance from Govt. of India is gratefully acknowledged. The authors PAK and CV also wish to acknowledge the Department of Science and Technology Unit on Nanoscience, IIT Madras for help in recording high resolution transmission electron micrographs.

References

1. D. Cotter, M.G. Burt, R.J. Manning, Phys. Rev. Lett. **68**, 1200 (1998)
2. G.P. Banfi, V. Degiorgio, D. Ricard, Adv. Phys. **47**, 447 (1998)
3. J. He, W. Ji, G.H. Ma, S.H. Tang, E.S.W. Kong, S.Y. Chow, X.H. Zhang, Z.L. Hua, J.L. Shi, J. Phys. Chem. B **109**, 4373 (2005)

4. W. Jia, E.P. Douglas, F. Guo, W. Sun, Appl. Phys. Lett. **85**, 6326 (2004)
5. N. Venkatram, D. Narayana Rao, M.A. Akundi, Opt. Express **13**, 867 (2005)
6. K.S. Bindra, A.K. Kar, Appl. Phys. Lett. **79**, 3761 (2001)
7. R.A. Vaia, J.F. Maguire, Chem. Mater. **19**, 2736 (2007)
8. K.I. Winey, R.A. Vaia (eds.,) *Polymer Nanocomposites*, (MRS Bulletin, Materials Research Society, Pittsburgh, PA, 2007)
9. H.P. Li, C.H. Kam, Y.L. Lam, W. Ji, Opt. Commun. **190**, 351 (2001)
10. AlL. Efros, A.L. Efros, Sov. Phys. Semicond. **16**, 772 (1982)
11. U. Woggon, *Optical Properties of Semiconductor Quantum Dots* (Springer, Berlin, 1997)
12. P. Nandakumar, C. Vijayan, Y.V.G.S. Murty, J. Appl. Phys. **91**, 1509 (2002)
13. C.B. Murray, D.J. Norris, M.J. Bawendi, J. Am. Chem. Soc. **115**, 8706 (1993)
14. D.J. Norris, Al.L. Efros, M. Rosen, M.G. Bawendi, Phys. Rev B **53**, 16347 (1996)
15. M.C. Klein, F. Hache, D. Ricard, C. Flytzanis, Phys. Rev. B **42**, 11123 (1990)
16. Al.L. Efros, A.I. Ekimov, F. Kozlowski, V. Petrova-Koch, H. Schmidbaur, S. Shumilov, Solid State Commun. **78**, 853 (1991)
17. Y. Wang, W. Mahler, Opt.Commun. **61**, 233 (1987)
18. P. Nandakumar, C. Vijayan, Y.V.G.S. Murty, Opt.Commun. **185**, 457 (2000)
19. Y. Wang, A. Suna, J. McHugh, E.F. Hilinski, P.A. Lucas, R.D. Johnson, J. Chem. Phys. **92**, 6927 (1990)
20. H. Yao, S. Takahara, H. Mizuma, T. Kozeki, T. Hayashi, Jpn. J. Appl. Phys. part 1 **35**, 4633 (1996)
21. T. Miyoshi, N. Matsuo, P. Maly, F. Trojanek, P. Nemec, J. Kudrna, J. Mater. Sci. Lett. **20**, 343 (2001)
22. V. Klimov, P. Haring Bolivar, H. Kurz, Phys. Rev. B **53**, 1463 (1996)
23. V.I. Klimov, Ch.J. Schwarz, D.W. Mcbranch, Phys. Rev. B **60**, R2177 (1999)
24. J. He, W. Ji, G.H. Ma, S.H. Tang, E.S.W. Kong, S.Y. Chow, X.H. Zhang, Z.L. Hua, J.L. Shi, J. Phys. Chem. B **109**, 4373 (2005)
25. R.E. Schwerzel, K.B. Spahr, J.P. Kurmer, V.E. Wood, J.A. Jenkins, J. Phys. Chem. A **102**, 5622 (1998)
26. H. Du, G.Q. Xu, W.S. Chin, L. Huang, W. Ji, Chem. Mater. **14**, 4473 (2002)
27. P.A. Kurian, C. Vijayan, C.S. Suchand Sandeep, R. Philip, K. Sathiyamoorthy, Nanotechnology **18,** 075708 (2007)
28. A. Rosencwaig, A. Gersho, J. Appl. Phys. **47**, 64 (1977)
29. M. Sheik-Behae, A.A. Said, T.M. Wei, D.J. Hagan, E.W. Van Stryland, IEEE J. Quantum Electron **26**, 760 (1990)
30. Y.V.G.S. Murti, P. Nandakumar, C. Vijayan, Phys. Educ. **16**, 229 (1999)
31. Y. Wang, N. Herron, Phys. Rev. B **42**, 7253 (1990)
32. P.E. Lippens, M. Lanoo, Phys. Rev. B **39**, 10935 (1989)
33. S.V. Nair, L.M. Ramaniah, K.C. Rustagi, Phys. Rev. B **45**, 5969 (1992)
34. P. Nandakumar, A.R. Dhobale, Y. Babu, M.D. Sastry, C. Vijayan, Y.V.G.S. Murti, K. Dhanalakshmi, G. Sundararajan, Solid State Commun. **106**, 193 (1998)
35. Y. Gao, X. Zhang, Y. Li, H. Liu, Y. Wang, Q. Chang, W. Jiao, Y. Song, Opt. Commun. **251**, 429 (2005)
36. E.F. Hilinski, P.A. Lucas, Y. Wang, J. Chem. Phys. **89**, 3435 (1988)
37. K. Misawa, H. Yao, T. Hayashi, T. Kabayashi, Chem. Phys. Lett. **183**, 113 (1991)